Ecological Indicators 130 (2021) 108033

Contents lists available at ScienceDirect

Ecological Indicators

journal homepage: www.elsevier.com/locate/ecolind

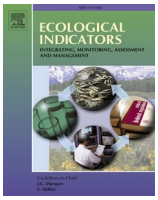

Decadal increase in the ecological status of a North-Atlantic intertidal seagrass meadow observed with multi-mission satellite time-series

Maria Laura Zoffoli [a,*], Pierre Gernez [a], Laurent Godet [b], Steef Peters [c], Simon Oiry [a], Laurent Barillé [a]

[a] Université de Nantes, Laboratoire Mer Molécules Santé, Faculté des Sciences, 2 rue de la Houssinière, 44322 Nantes, France
[b] CNRS, Université de Nantes, UMR LETG, B.P. 81223, 44312 Nantes, France
[c] Water Insight, 6709 PG 22 Wageningen, the Netherlands

ARTICLE INFO

Keywords:
Water Framework Directive
Interannual variability
Ecosystem monitoring
Earth Observation
Recovery
Zostera noltei
Zostera noltii

ABSTRACT

Seagrass meadows are monitored in the frame of several environmental programs worldwide, including the Water Framework Directive (WFD), to evaluate the ecological status of European coastal and transitional water bodies. The large size, spatial complexity, and interannual variability of seagrass ecosystems significantly challenge field monitoring. In this study, a multi-mission satellite time-series was used to estimate long-term changes in seagrass status in a macrotidal system dominated by *Zostera noltei*, at Bourgneuf Bay (French Atlantic coast). Metrics of seagrass extent and density were obtained from Earth Observation (EO) using validated and inter-calibrated Landsat, SPOT and Sentinel2 data from 1985 to 2020. The information provided by satellite data made it possible to compute and compare several seagrass indicators currently in use in several European countries (France, Portugal and UK) within the WFD. Both the seagrass extent and meadow-averaged density displayed increasing trends since 1985. A time-series of merged observations from various satellites revealed a high degree of interannual variability in seagrass extent, with abrupt losses (up to 50% within one year) alternating with periods of slow recovery (typically 4–6 years). The seagrass meadow which was in a moderate status (*sensu* the WFD) in the 1980s, achieved an overall recurrent good or high status since the mid-1990s. Altogether, the methods and results presented here demonstrated that EO is a reliable source of information for mapping and assessing the status of intertidal seagrass, complementing *in situ* measurements by providing long-term, spatial view and standardized observation framework. We recommend the systematic use of EO time-series in complement to traditional field measurements in seagrass monitoring programs such as the WFD.

1. Introduction

Seagrass meadows provide a wide range of ecosystem functions but are sensitive to the combination of direct anthropogenic impacts such as mechanical damage due to land reclamation, construction building, boat mooring and anchoring, alteration of sediment dynamics due to dredging and coastal engineering (Orth et al., 2006; Walker and McComb, 1992), together with indirect pressures resulting from global warming and sea-level rise (Valle et al., 2013). In addition, the global decline of natural vegetation reported for coastal watersheds, growing urbanization, as well as massive agricultural and industrial land use are responsible for pollution, land erosion, run-off, and seaward export of nutrients and contaminants causing eutrophication, degradation of water quality and transparency, enhanced sedimentation and hydromorphological changes, eventually impacting coastal ecosystems (Green et al., 2021; Short and Wyllie-Echeverria, 1996; Unsworth et al., 2019). Their recognized ecosystem value has motivated many studies to follow seagrass changes worldwide (de los Santos et al., 2019; Green et al., 2021; Kuo and Lin, 2010; Murphy et al., 2021; Shelton et al., 2017). While seagrass ecosystems at global scale have shown a decreasing trend since the 19th century (Green et al., 2021; Waycott et al., 2009), a reverse tendency has been reported since the 2000s in several European sites (de los Santos et al., 2019). Some authors attributed the regionally observed and recent expansions to local improvements in water quality, habitat remediation, or changes in coastal topography (Barillé et al., 2010; Bertelli et al., 2018; Calleja et al., 2017;

* Corresponding author.
E-mail address: laura.zoffoli@univ-nantes.fr (M.L. Zoffoli).

https://doi.org/10.1016/j.ecolind.2021.108033
Received 12 April 2021; Received in revised form 22 July 2021; Accepted 23 July 2021
Available online 10 August 2021

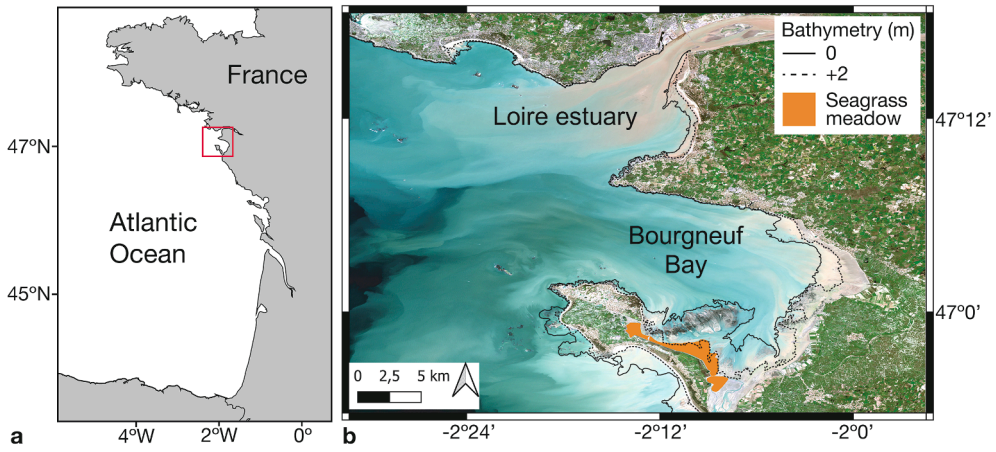

Fig. 1. Study area. Bourgneuf Bay (France) in the Atlantic coast (a) and the intertidal seagrass meadow adjacent to Noirmoutier island (b).

de los Santos et al., 2019; Román et al., 2020). Providing a consistent analysis of seagrass temporal changes is however very challenging due to large data gaps and spatiotemporal limitations in seagrass records (Unsworth et al., 2019), and the estimated trends vary among seagrass species, sites and time periods (de los Santos et al., 2019; Dunic et al., 2021; Green et al., 2021).

Concerned by the overall degradation of water quality, the European Union (EU) created a very ambitious program, the Water Framework Directive (WFD, 2000/60/EC), to monitor and evaluate the ecological status of inland, transitional (TWB), and coastal (CWB) water bodies up to 1 nautical mile. However, evaluating the ecological status of 111,062 water bodies using exclusively field observations turned out to be extremely challenging, and the status of many sites has still not been assessed (Papathanasopoulou et al., 2019). Amongst many ecological parameters, seagrass habitats have been chosen as WFD indicator due to their high sensitivity to natural and anthropogenic pressures. In particular, intertidal seagrass has been selected as a Biological Quality Element for the assessment of TWB and CWB ecological status (Foden, 2007). Three metrics are routinely included in the calculation of an Ecological Quality Ratio (EQR) used to determine a water body's quality status: (1) taxonomic composition (seagrass species richness); (2) bed extent (total surface occupied by the meadow); and (3) density (either seagrass shoots per square meter or seagrass percent cover) (Foden, 2007). However, even though intertidal seagrass beds are partially emerged during low tide, they are not easily accessible, and assessing their areal extent with conventional field sampling is very challenging, especially over meadows >1 km^2. Seagrass beds have complex shapes, with irregular boundaries, successions of patches and bare areas. Methods deploying GPS have been successfully used to delimit both intertidal and shallow subtidal seagrass beds (Young et al., 2012; Young et al., 2015) but are limited as scale increases. The great interannual variability of seagrass beds also require very regular field surveys (at least every year or every two years), which remains a very time-consuming exercise.

The synoptic capacity of Earth Observation (EO) can overcome these constraints. Satellite remote-sensing has a significant though underexploited potential to map many types of coastal environments, including seagrass beds (Klemas, 2013; Kovacs et al., 2018; Phinn et al., 2008; Roelfsema et al., 2014; Traganos and Reinartz, 2018a; Traganos and Reinartz, 2018b; Zoffoli et al., 2020). Since almost five decades, satellite missions such as Landsat and SPOT have acquired data at high spatial resolution (pixel size $\leq$ 30 m) over the whole planet. Today, we can benefit from satellite time-series to obtain a long-term view of coastal habitats' condition and to retrospectively document their evolution and dynamics (Knudby et al., 2010). Furthermore, not only seagrass beds but adjacent habitats can be taken into consideration due to the synopticity of satellite observation, providing a holistic view of coastal ecosystems that is fundamental for effective management (El Mahrad et al., 2020). There are plenty of examples of coastal studies demonstrating the usefulness of satellite imagery to document urban expansion (Chai and Li, 2018), land reclamation (Xu et al., 2021) river plumes evolution (de Rudorff et al., 2011), as well as temporal changes in coral reefs (Palandro et al., 2008), mangroves (Aljahdali et al., 2021), benthic macroalgae (Lõugas et al., 2020), and inter- and subtidal seagrass meadows (Barillé et al., 2010; Calleja et al., 2017; Dekker et al., 2005; El-Hacen et al., 2020; Hossain et al., 2015; León-Pérez et al., 2019; Lyons et al., 2013; McKenzie et al., 2020; Santos et al., 2020; Sousa et al., 2019).

To date, seagrass monitoring under the WFD is only based on data collected during field campaigns and/or combined with aerial photographs (Auby et al., 2018; Neto et al., 2013; UKTAG, 2014). Moreover, with a minimum requirement of a single survey every 6 years (Wilkes et al., 2017), the WFD sampling strategy is not adapted to accurately describe interannual variations in temporally dynamic seagrass beds. Interestingly, EO has the potential to fill up data gaps in these ecosystems and complement field measurements, in particular since the advent of the Sentinel2 (S2) mission (2015 – present), which acquires images at both high spatial (10 m) and temporal ($\leq$5 days) resolutions (Kohlus et al., 2020).

The objective of the present study is to take advantage of 36-year time-series of satellite observations (1985–2020) to document the interannual variability and temporal trends of an intertidal seagrass meadow over an Atlantic temperate coastal area (Bourgneuf Bay, France). First, the consistency of combining three multispectral satellite missions (Landsat, SPOT and S2) with different resolutions was demonstrated. Second, the meadow total extent was determined using 20 m satellite-derived maps of seagrass percent cover (SPC), a metric which allowed us to identify the densest and most resilient seagrass areas within the whole meadow. Finally, the seagrass ecological status was evaluated using satellite data, adapting the methods routinely applied by three different Member States (MS), namely France, Portugal and UK, in the frame of the WFD seagrass monitoring. The method proposed here, based on remote sensing, seeks to evaluate the evolution of meadow surfaces in the long term and understand how it can provide information on the health status of coastal ecosystems.

2. Material and methods

2.1. Study area

The intertidal seagrass bed analyzed in this study is one of the French meadows selected for the WFD monitoring of the seagrass indicator (Auby et al., 2018). The meadow is dominated by *Zostera noltei* and localized in the French Atlantic coast (47°N, 2°05′W), south to the Loire Estuary (Fig. 1). Some small isolated stands of *Zostera marina* can be also found close to oyster-farming sites (Barillé et al., 2010). The intertidal

Table 1
Summary of SPOT/S2 and Landsat low-tide data available during the seasonal maximum development of *Z. noltei*.

	SPOT/S2 images	Landsat images
Time period	1988–2020	1985–2020
Number of images	20	25
Original pixel size (m)	10 or 20	30
Atmospheric correction	SMAC	Landsat 5–7: LEDAPS

area presents a high tidal range (6 m during spring tides) and the seagrass meadow is fully emerged during low tide. The bay is a semi-enclosed system, protected from waves by the Noirmoutier island in the south, with a highly turbid water column (suspended particulate matter can exceed 300 g m^{-3}; Gernez et al., 2014) and a strong accumulation of fine fraction sediments on the seabed (Sanchez, 2008). In this temperate latitude, *Z. noltei* presents a seasonal cycle with a late summer maximum and a minimal coverage (if not a total disappearance) of above-ground biomass in winter (Zoffoli et al., 2020).

2.2. Satellite data and processing

2.2.1. Creation of a consistent database

Three satellite datasets were compiled to create a consistent time-series of seagrass maps from 1985 to 2020 in Bourgneuf Bay (Table 1). The first dataset was obtained from Landsat5 and 7 (1985–2020), the second from Satellite Pour l'Observation de la Terre (SPOT1-5) (1988–2013), and the third from Sentinel2 (S2, 2015–2020). As S2 was specifically designed to improve and ensure consistency and continuity with the SPOT mission (Hagolle et al., 2015), the SPOT and S2 data were grouped together. SPOT and S2 provide images at high spatial resolution (pixel size is 10 or 20 m depending on the satellite). The SPOT and S2 time-series were used as the core component of the long-term analysis of the seagrass dynamics because this resolution makes it possible to quantitatively describe the seagrass meadow spatial structure (Zoffoli et al., 2020). Due to its lower spatial resolution of 30 m, the Landsat imagery was not primarily used in spatial analyses. However, the Landsat time-series was useful to check the consistency of the SPOT and S2 atmospheric correction, and to fill the gaps in the SPOT and S2 time-series because of its long duration and processing stability.

2.2.2. Satellite images selection

Several constraints were applied to ensure an optimal satellite observation of intertidal seagrass meadows (Zoffoli et al., 2020). First, the images had to be acquired during low tide so that the meadow was fully emerged. Here, the tidal information provided by the *Service Hydrographique et Océanographique de la Marine* (SHOM) was used as a reference (water height < 3 m at the nearest harbor of L'Herbaudière). Second, the images had to be acquired during the annual peak of the meadow's development to limit the influence of seasonal variability (Zoffoli et al., 2020). An analysis of the full Landsat archive allowed us to determine that the optimal temporal window corresponding to the seagrass maximum development occurred between 24/Jul and 15/Oct (see Appendix A for more details). Last, only cloud-free images were selected. A total number of 45 Landsat, SPOT, and S2 images were eventually available from 1985 to 2020 (Table 1).

2.2.3. Processing of SPOT and S2 images

SPOT images were downloaded from the SPOT World Heritage (https://www.theia-land.fr/). S2 images were downloaded from the Copernicus Open Access Hub (https://scihub.copernicus.eu/). Both SPOT and S2 images were downloaded as top-of-atmosphere (TOA) reflectance data. The same atmospheric correction was applied for SPOT and S2 using the Simplified Model for Atmospheric Correction (SMAC; Rahman and Dedieu, 1994; available at https://labo.obs-mip.fr/multitemp/) to compute the bottom-of-atmosphere reflectance (R). A summer average of the aerosol optical thickness (AOT) over the site equal to 0.1 was used.

The normalized difference vegetation index (NDVI; Tucker, 1979) was used to detect the seagrass meadows. The NDVI is computed from the relative difference between the reflectance in the near-infrared (NIR) and the red spectral regions (Eq. (1)). It has been widely used for vegetation remote sensing in many contexts, including intertidal primary producers (Barillé et al., 2010; Brito et al., 2013; Méléder et al., 2020; Valle et al., 2015; van der Wal et al., 2010). As the spectral resolutions of SPOT (NIR band at 840 nm, and red band at 645 nm) and S2 (NIR and red bands at respectively 842 and 665 nm) are not the same, the $NDVI_{SPOT}$ was recalibrated to $NDVI_{S2}$ to avoid sensor bias (Zoffoli et al., 2020). Similarly, all SPOT and S2 NDVI images were resampled to the same spatial resolution (20 m), using the nearest neighbour resampling method.

$$NDVI = \frac{R_{NIR} - R_{Red}}{R_{NIR} + R_{Red}} \quad (1)$$

A radiometric mask ($0.129 \leq NDVI < 0.8$) was applied to remove flooded areas and drifted macroalgae, and to select only emerged seagrass (Barillé et al., 2010; Zoffoli et al., 2020). The above-ground seagrass percent cover (SPC) was then computed from the NDVI using a relationship specifically calibrated and validated for intertidal meadows of *Z. noltei* located along the European Atlantic coast (Eq. (2); from Zoffoli et al., 2020).

$$SPC = 172.06 \bullet NDVI - 22.18 \quad (2)$$

Terrestrial areas and those corresponding to rocky shores or below the bathymetric line of + 2 m were masked to select only the seagrass meadow.

2.2.4. Processing of Landsat images

Landsat images were downloaded from the United States Geological Survey (USGS) portal (EROS science processing architecture on demand interface - ESPA), https://espa.cr.usgs.gov/) as ground surface NDVI product. The $NDVI_{Landsat}$ was recalibrated to $NDVI_{S2}$ (Zoffoli et al., 2020) and SPC was computed similarly as for SPOT and S2 (Eq. (2)). Due to its long-term stability, the Landsat dataset was used to assess the consistency of the SPOT/S2 time-series. The comparison was performed over 4 types of targets commonly found in temperate intertidal areas: sandy beach, bare sediment adjacent to the seagrass meadow, macroalgae, and seagrass (see Appendix B for more details). The reason for selecting different intertidal targets was to cover a wide range of NDVI values, from low values represented by sandy beach and bare sediment, to the highest values represented by macroalgae, then, providing a comparison for the largest dynamic range of the index. Only for satellite intercomparison purposes, SPOT and S2 has been resampled to 30 m pixel size to be compatible with Landsat spatial resolution. The final 36-year long merged time-series was composed by 29 satellite images (SPOT, S2 and Landsat) acquired from 1985 to 2020 (Table B1), with a maximum gap of 3 years between each image.

2.3. Seagrass percent cover and density metrics

A large diversity of seagrass indicators has been developed to evaluate the ecological status of TWB and CWB in all European countries (Marbà et al., 2013). As suggested by Papathanasopoulou et al. (2019), remote sensing has the potential to harmonize the diverse national methods because several seagrass metrics, including bed extent and density, can be consistently computed from satellite-derived maps of seagrass percent cover. The estimation of the meadow total surface is generally computed as the extent of all areas with SPC $\geq$ 20%. This threshold has been empirically selected to distinguish seagrass from bare sediment (Dolch et al., 2017; Valle et al., 2015) and/or biofilms of benthic microalgae (Barillé et al., 2010). The same threshold is also applied to airborne images to reduce measurement uncertainties (Reise and Kohlus, 2008). As the detection accuracy improves with seagrass density, two additional metrics corresponding to the areas of dense and very dense seagrass cover (respectively corresponding to SPC $\geq$ 50%,

Table 2
Ecological Quality Ratios (EQR) intervals used to define the ecological status based on seagrass indicator, according to each Member State (Neto et al., 2018).

EQR_{FR}	EQR_{UK}	EQR_{PT}	Ecological status
$1 \geq EQR > 0.8$	$1 \geq EQR > 0.8$	$1 \geq EQR > 0.8$	High
$0.8 \geq EQR > 0.645$	$0.8 \geq EQR > 0.607$	$0.8 \geq EQR > 0.60$	Good
$0.645 \geq EQR > 0.4$	$0.607 \geq EQR > 0.4$	$0.60 \geq EQR > 0.4$	Moderated
$0.4 \geq EQR > 0.2$	$0.4 \geq EQR > 0.2$	$0.4 \geq EQR > 0.2$	Poor
$0.2 \geq EQR \geq 0$	$0.2 \geq EQR \geq 0$	$0.2 \geq EQR \geq 0$	Bad

Table 3
Scaling factors used to compute the EQR_E and EQR_D from the relative deviation to the reference (Auby et al., 2018).

ΔD or ΔE (%)	EQR_D or EQR_E
0–10	1–0.80
11–17	0.79–0.66
18–30	0.65–0.50
31–50	0.49–0.30
51–100	0.295–0

and SPC $\geq$ 80%) were recently proposed to improve the robustness of satellite-derived interannual analysis (Calleja et al., 2017; Zoffoli et al., 2020). In summary, the following seagrass metrics were computed from the merged time-series: total extent (SPC $\geq$ 20%), and area of sparse (20% $\leq$ SPC $<$ 50%), dense (50% $\leq$ SPC $<$ 80%) and very dense cover (80% $\leq$ SPC). Surfaces of the different SPC categories were estimated based on a map reprojection to the RGF 93 / Lambert-93 (EPSG: 2154) coordinate reference system. In addition, the meadow-averaged seagrass density was estimated from all pixels with SPC $\geq$ 20%.

The rate of change (μ) was estimated for the seagrass surface and for the meadow-averaged density (Waycott et al., 2009):

$$\mu = 100 \bullet \left(\frac{\ln(A_2) - \ln(A_1)}{t_2 - t_1} \right) \quad (3)$$

where A_2 and A_1 correspond to the seagrass surface (or density) values at times t_2 and t_1 respectively.

2.4. Seagrass EQR and ecological status under the WFD

The intertidal seagrass Ecological Quality Ratio (EQR) was computed from 1985 to 2020 following methods currently applied within the WFD. The computation of the EQR differs within Member States. Here, we applied to the satellite dataset the method used in France (EQR_{FR}, Auby et al., 2018), in Portugal (EQR_{PT}, Neto et al., 2013), and in the United Kingdom (EQR_{UK}, UKTAG, 2014). Independently of the method, the EQR always integrates three structural metrics: seagrass total surface (*E*), density (*D*, usually indexed by SPC; Dolch et al., 2013; Foden, 2007; UKTAG, 2014), and taxonomy (*T*). The metrics *E* and *D* were estimated from satellite data. For the metric *T*, we considered the maximum invariant value during the 36-year period due to the permanent presence of *Z. noltei* and *Z. marina* reported in the site (Gruet, 1976; Bargain, 2012). To estimate each metric, the WFD also considers a reference that theoretically corresponds to the maximal potential of each metric during undisturbed pristine conditions or during minimal disturbance. In practice, the reference is considered as the year with the largest extension or densest meadow (Foden and Brazier, 2007). We considered 2002 and 2020 as years of reference for the metrics *E* and *D*, respectively, as they presented the highest values. Finally, the seagrass ecological status was computed from the EQR (Table 2).

2.4.1. France's method

For each individual year, the relative loss in seagrass density was computed with respect to the reference (and similarly for *E*) using:

$$\Delta D(\%) = 100 \bullet \frac{|D_{ref} - D|}{D_{ref}} \quad (4)$$

where the suffix "ref" corresponds to the metric for the year of reference.

The relative deviations of seagrass density and extent were then used to compute the density (EQR_D) and extent (EQR_E) ecological quality ratios using scaling factors (Table 3) (Auby et al., 2018). In the case of the EQR_T, the French method considers a value of 1 if no changes were observed in the taxonomic composition of the seagrass meadow. Finally, the EQR_{FR} was estimated as the average of the *D*, *E* and *T* ecological quality ratios:

$$EQR_{FR} = \frac{(EQR_D + EQR_E + EQR_T)}{3} \quad (5)$$

2.4.2. UK's method

As in France, the UK method (UKTAG, 2014) is based on the relative deviation from the reference for the density and extent metrics (Eq. (4)). However, it considers different intervals of percent of loss and another additional and more sophisticated method to rescale Δ into 0 – 1 values (UKTAG, 2014). In the case of EQR_T, UK's method attributes a value of 0.9 if no changes were detected. The final EQR_{UK} was also computed as the average of EQR_D, EQR_E and EQD_T.

2.4.3. Portugal's method

The Portuguese method (Neto et al., 2013) differs from the two other ones. For each metric, the EQR is computed as the ratio of the value of the considered year to the reference. The final EQR was computed using different weights for the metrics *D*, *E* and *T*:

$$EQR_{PT} = \left(\frac{D}{D_{ref}}\right) \bullet 0.5 + \left(\frac{E}{E_{ref}}\right) \bullet 0.3 + \left(\frac{T}{T_{ref}}\right) \bullet 0.2 \quad (6)$$

2.5. Statistical analysis

2.5.1. Matchups, datasets comparison and trend analysis

The performance of the SMAC atmospheric correction was analyzed using field reflectance measurements collected in 2009, 2018, and 2019 over different intertidal targets in Bourgneuf Bay. Match-ups were performed for individual bands along the visible and NIR regions, and for NDVI, and evaluated in terms of root mean square difference (RSMD, Eq. (7)), unbiased absolute percent difference (UAPD, Eq. (8)) and by fitting to a linear model.

$$RMSD = \sqrt{\sum_{i=1}^{N} \frac{\left(x_{modelled,i} - x_{insitu,i}\right)^2}{N - 1}} \quad (7)$$

$$UAPD = 2 \bullet \frac{\left|x_{modelled,i} - x_{insitu,i}\right|}{\left(x_{modelled,i} + x_{insitu,i}\right)} \bullet 100 \quad (8)$$

where $x_{modelled,i}$ and $x_{insitu,i}$ corresponded to modeled or observed data respectively, and *N* corresponded to the sample size.

Satellite intercomparison was performed on NDVI values extracted over four different target types: sandy beach, intertidal sediment, seagrass, and macroalgae. SPOT and S2 samples were compared with Landsat and a linear model was adjusted and compared its slope with the slope of the $y = x$ relationship through a covariance analysis (ANCOVA). Differences between the two datasets were computed through UAPD and RMSD.

The stability of the NDVI time-series was evaluated over the most stable targets, namely macroalgae and sediment, using the coefficient of variation (CV; Eq. (9)).

$$CV(\%) = \frac{\sigma}{\bar{x}} \bullet 100 \quad (9)$$

where $\bar{x}$ and σ are the mean and standard deviation respectively.

The long-term trends were analyzed by linear regression. Any change from a slope equal to zero was tested with ANCOVA. The trends were

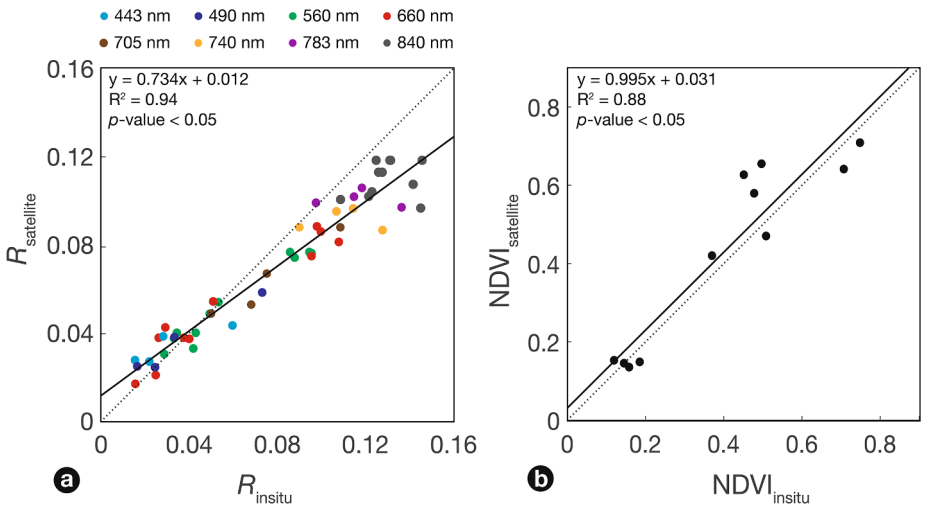

Fig. 2. *In situ* validation of the SMAC atmospheric correction for SPOT (2009) and S2 (2018 and 2019) for (a) reflectance ($R_{satellite}$) in the visible and NIR regions, and (b) NDVI. Dotted lines correspond to 1:1 slope while black lines correspond to the linear regression.

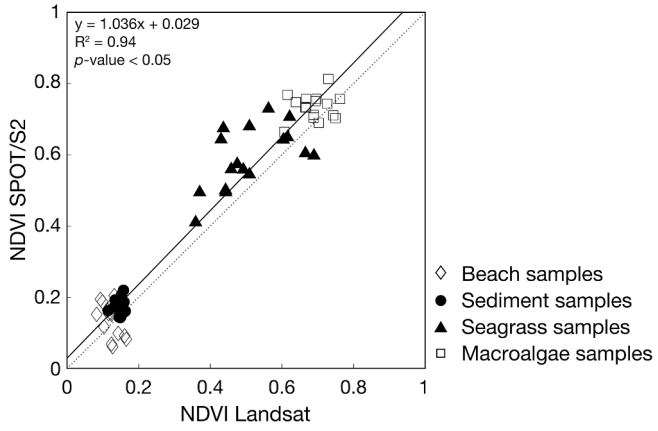

Fig. 3. Comparison of the SPOT/S2 and Landsat NDVI. The comparison was performed over four common types of intertidal targets: beach (diamonds), sediment (circles), seagrass (triangles) and macroalgae (squares). Dotted line corresponds to 1:1 slope while black line corresponds to the linear regression.

separately computed from the SPOT/S2 and merged datasets, and compared through ANCOVA analyses. All statistical analyses were performed using the MATLAB software.

The differences between EQR estimated from the three methods (French, British and Portuguese) were compared with a non-parametric repeated measures Friedman test and *a posteriori* pairwise Wilcoxon rank test. Ecological status categories (high, good, moderated, poor, bad) were reclassified to 5, 4, 3, 2, 1 and compared with the same statistical tests.

2.5.2. Analysis of seagrass spatial structure

The seagrass ecological status was computed using spatially-averaged metrics of the whole meadow. While such proxies are useful for time-series analysis, they do not allow study of the changes in the meadow's spatial distribution. More evolved spatial statistics such as landscape metrics have proved useful to provide a spatialized picture of the temporal changes in benthic ecosystems (Godet et al., 2011; Lyons et al., 2013; Santos et al., 2016). Here, as a first attempt to characterize the landscape dynamics of the meadow, we performed a frequency analysis of the dense seagrass patches. Using the SPOT and S2 time-series we computed a frequency map where each pixel corresponds to the number of occurrences of SPC $\geq$ 50% from 1988 to 2020. Due to its coarser spatial resolution (30 m), Landsat data were not used for this spatial analysis.

3. Results

3.1. In situ validation and time-series consistency

The satellite-derived surface reflectance was compared with *in situ* measurements to assess the accuracy of satellite observations. The SPOT/S2 and *in situ* reflectance measurements were correlated in the visible and NIR regions, with a slight underestimation in the visible bands and an overestimation in the NIR bands ($R^2 = 0.94$, p-value < 0.05, RMSD $= 0.008$, and mean UAPD of 17.2%; Fig. 2a). These differences did not impact the NDVI, for which the comparison between *in situ* and satellite measurements was very close to the 1:1 line ($R^2 = 0.88$, p-value < 0.05, RMSD $= 0.088$ and mean UAPD of 16.1%; Fig. 2b).

The comparison of SPOT/S2 and Landsat NDVI demonstrated the consistency of the merged satellite datasets over seagrass beds as well as over other common types of intertidal habitats ($R^2 = 0.94$, p-value < 0.05, RMSD $= 0.062$ and mean UAPD of 14.6%; Fig. 3). A linear relationship was obtained between SPOT/S2 and Landsat, with a slope not significantly different from 1 (p-value > 0.05) and a small intercept ($NDVI_{SPOT/S2} = 1.036 \cdot NDVI_{Landsat} + 0.029$). The bias due to the non-negligible intercept was corrected by adding an offset of 0.029 to $NDVI_{Landsat}$.

The stability of the satellite time-series was assessed over areas covered by dense and permanent macroalgae, or corresponding to bare sediment. The NDVI was stable over macroalgae (CV was 4.8% for SPOT/S2 and 6.5% for Landsat) and sediment (CV of 12.3% and 8.1% for SPOT/S2 and Landsat respectively). Due to the temporal stability of the NDVI time-series over these two independent references (non-significant linear fit, with p-value > 0.05; comparison of datasets through ANCOVA analyses with p-value > 0.05), we assumed that our analysis of temporal changes in seagrass was neither biased by instrumental nor processing issues.

Pairwise comparisons of the temporal trend in seagrass extent estimated from the SPOT/S2 and from the SPOT/S2 + Landsat merged-time series did not show any significant differences (ANCOVA analyses with p-values > 0.05). Overall, these results demonstrated the temporal consistency of the various satellite datasets. Using Landsat to fill gaps in the SPOT/S2 time-series did not bias temporal trends.

3.2. Changes in seagrass extent and density

The merged time-series covered 36-years of seagrass variation in Bourgneuf Bay. A satellite image was almost available every year from 1985 to 2020, and the longest gap in the series was 3 years (from 1998 to 2001). Since S2 launch in 2015, the series was uninterrupted. The changes in cover were characterized by complex spatial patterns and a

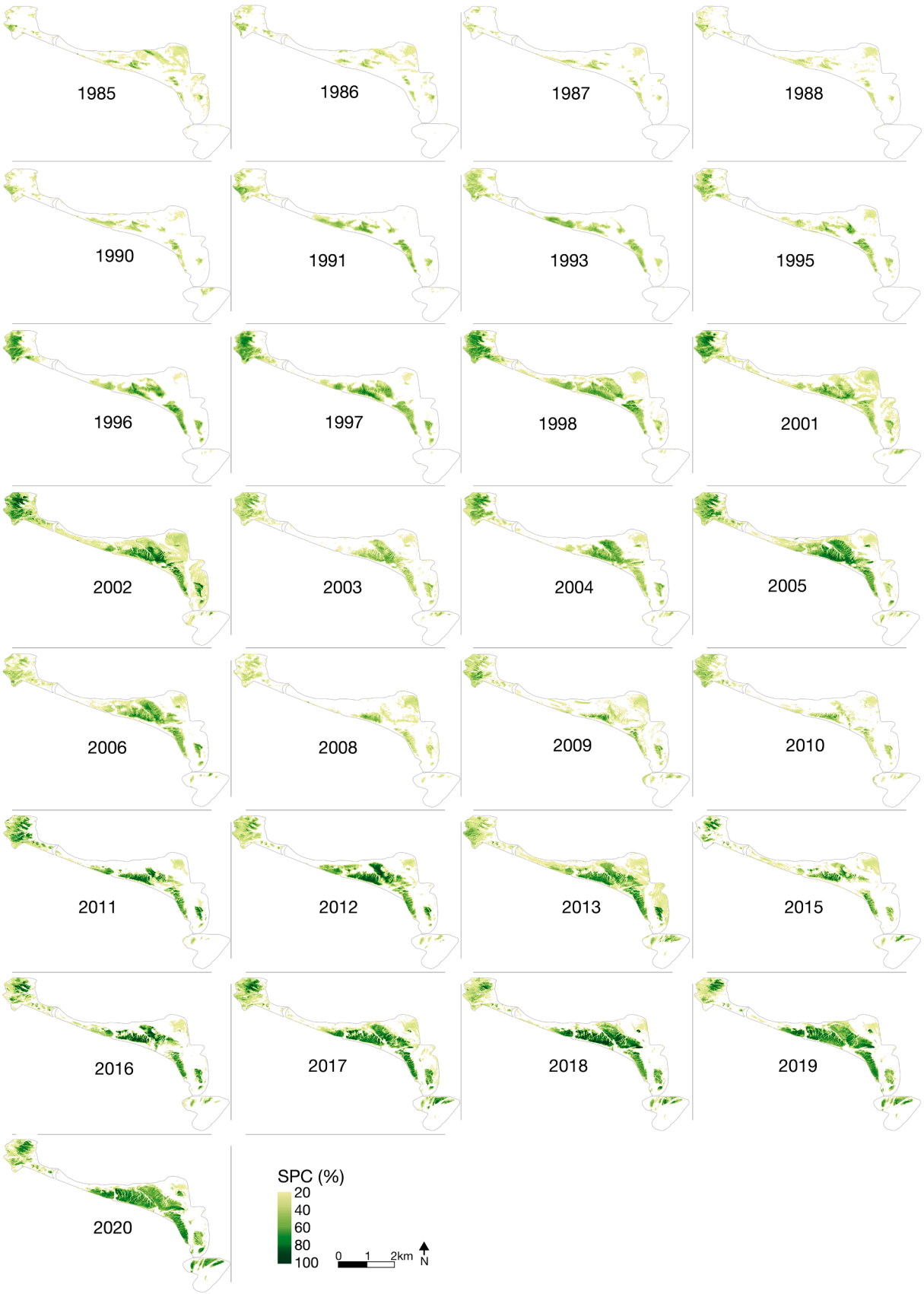

Fig. 4. Time-series of intertidal *Z. noltei*-dominated seagrass beds Bourgneuf Bay derived from Landsat, SPOT and S2 observations from 1985 to 2020. The maps show the seagrass percent cover (SPC). Pixels with SPC < 20% were masked.

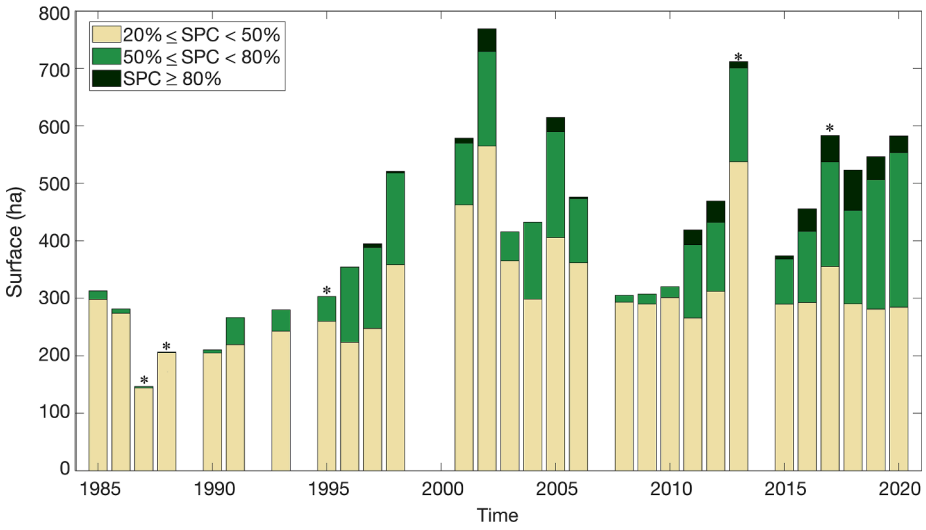

Fig. 5. Satellite-derived time-series of seagrass extent in Bourgneuf Bay from 1985 to 2020, for three classes of seagrass percent cover (SPC): 20% ≤ SPC < 50%, 50% ≤ SPC < 80% and SPC ≥ 80%. The seagrass extent was computed during the late summer seasonal maximum. The * mark indicates the cases when no satellite image was available during the optimal temporal window and for which the seagrass extent would be subjected to a seasonal bias (Appendix A).

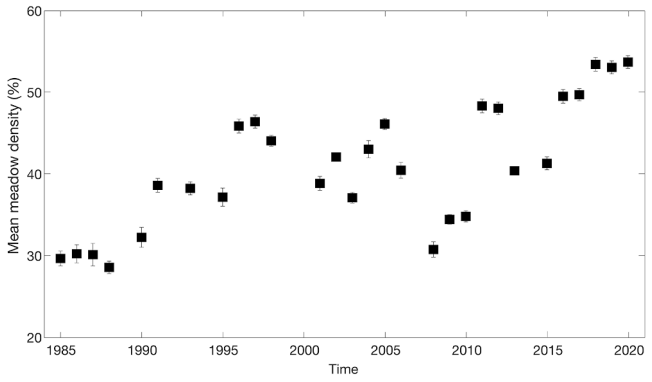

Fig. 6. Satellite-derived time series of the meadow-averaged seagrass density in Bourgneuf Bay from 1985 to 2020. The mean percent cover was computed from all pixels with SPC ≥ 20%. The vertical error bars show confidence interval at 5% ($\overline{x} \pm 1.96 \cdot \sigma/\sqrt{N}$).

very high interannual variability (Fig. 4). Overall, the seagrass extent increased since 1985 (significant linear fit with *p*-values < 0.05, and positive slope statistically different from zero,$y = 8.62 \cdot x - 16844$, $R^2 = 0.37$). The satellite observation made it possible to assess the temporal variability over different classes of seagrass cover (Fig. 5). Interestingly, the temporal dynamics varied with the level of cover: the extent of the whole meadow (corresponding to SPC ≥ 20%) and of the dense meadow (SPC ≥ 50%) increased, but the area of sparse cover (20% ≤ SPC ≤ 50%) did not present any significant trend. The long-term increase in seagrass extent can therefore be mostly attributed to the expansion of the densest seagrass patches. From 1985 to 2020, the mean rate of change was 2.4 and 9.3% yr^{-1} for the whole and dense meadow, respectively.

The changes were neither spatially nor temporally homogeneous, and the seagrass showed fluctuating patchy patterns over the years (Figs. 4 and 5). The 1980s and early 1990s corresponded to the lowest extension and a dominance of sparse cover. Over this period, the extent of the whole and dense meadow was always lower than 400 and 100 ha respectively. Since the mid-1990s, an increase in both seagrass extent and density has been occurring, and the extent of the whole and dense meadow exceeded a few times 700 and 250 ha, respectively. While an overall expansion has been observed over the last 25 years, several events of decline occurred in 2003, 2008/2010 and 2015. The losses were both very rapid and severe, and as much as 50% of the seagrass extension could be lost in only one year (Fig. 5). The losses were generally followed by periods of recovery. The pace of recuperation was however slower than the rate of loss, and the meadow generally recovered in about 3–6 years (in 1995–1998, 2004–2006, 2011–2013, and 2015–2020). The maximum extent of the whole meadow occurred in 2002 (769 ha), whereas the maximum extent of the dense meadow was in 2020 (327 ha). During the last four years (2017–2020), an unprecedented situation was observed during which the meadow displayed a dominance of the densest classes, *i.e.,* >50% of the seagrass extent corresponded to SPC ≥ 50% (Fig. 5).

The temporal changes in the meadow-averaged density (in terms of seagrass percent cover) were similar to that of the seagrass extent (Fig. 6). An increasing trend was observed from 1985 to 2020 (significant linear fit with *p*-value < 0.05, and positive slope statistically different from zero; $y = 0.51 \cdot x - 978.2$, $R^2 = 0.53$), with an overall rate of change of 1.3% yr^{-1}. The mean density was lower than 31% during the beginning of the series in the 1980s, and higher than 52% during the three last years (2018–2020). The mean density was correlated to the extent of the dense seagrass meadow (linear fit, $R^2 = 0.85$, *p*-value < 0.05), and the periods of decline and recovery were synchronous for the extent and density metrics.

3.3. Analysis of spatial changes

Using a frequency analysis, we identified the most resilient seagrass clusters, corresponding to the areas where a dense cover (SPC ≥ 50%) was observed during at least 50% of the years from 1988 to 2020 (Fig. 7). The main kernels were identified in the northwestern and central parts of the meadow, representing about 40% of the seagrass total extent. The northwestern patch was quite small and fragmented, whereas the central kernels were larger and more continuous. No kernel areas were identified in the southeastern part of the meadow. In Bourgneuf Bay, the seagrass meadow occurs between the + 2 and + 4 isobaths. The lower boundary of the more frequently dense areas corresponded to the contour of the + 2.75 m bathymetric line.

3.4. Seagrass ecological status

The seagrass ecological status varied from moderate to high all over the 1985–2020 time-series. An increasing trend was observed, with years of decline alternating with periods of recovery, as previously described for the seagrass extent and mean density (Fig. 8). The meadow

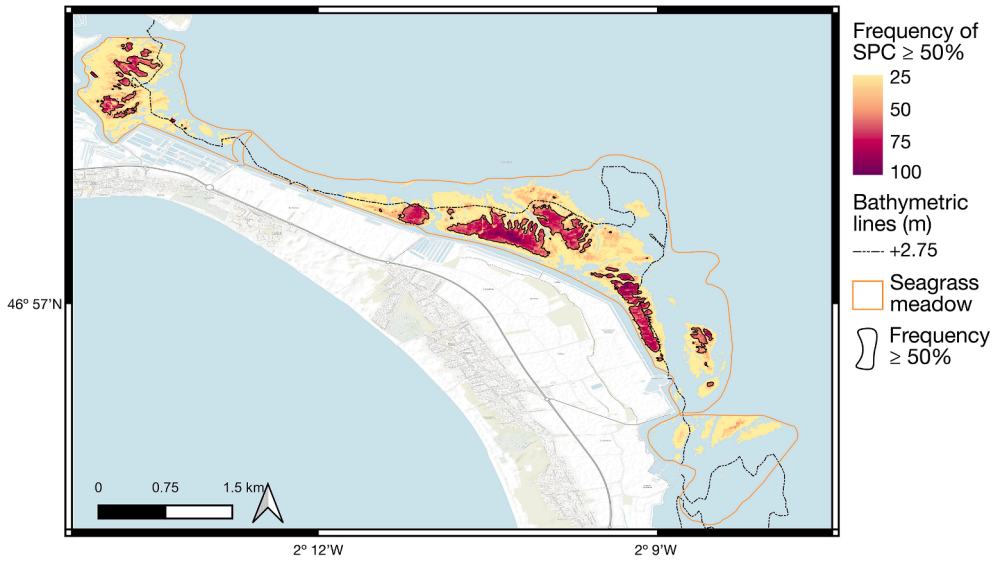

Fig. 7. Frequency of occurrence (in %) of dense seagrass cover (SPC ≥ 50%) derived from the SPOT/S2 dataset from 1988 to 2020.

was in a moderate status in the 1980s. Since the mid-1990s, the meadow was mostly in a good or high status, with the exception of few years. Even during periods of decline, the seagrass status did not fall below moderate. Satellite observations made it possible to quantitatively compare the metrics of three countries along 36 years. There was an overall agreement between the patterns displayed by the three methods. However, there were significant differences between the three methods, both for EQR (Friedman test, p-value < 0.05) and ecological status (Friedman test, p-value < 0.05). The status using the French method was the lowest, whereas the status using the Portuguese method was the highest. Status from the three methods matched in approximately 50% of the years. From 1985 to 2020, the FR and UK ecological status did not show significant differences (p-value $= 0.6$); but the UK and PT, as well as the FR and PT status showed significant differences (pairwise Wilcoxon, p-value < 0.05 in both cases).

4. Discussion

4.1. Recommendations for seagrass monitoring programs

In France, the 12 intertidal meadows of *Z. noltei* monitored within the WFD (Auby et al., 2018) are all large enough to be observed with S2. However, a limited number of sites (only 2 over 12) has been investigated using satellite images (Barillé et al., 2010; Froidefond et al., 2012; Zoffoli et al., 2020). By documenting seagrass dynamics in one of the WFD French sites, the present study aims to demonstrate the advantages of using EO for monitoring seagrass status. The systematic use of EO in complement to field surveys would make it possible to more accurately document the status of intertidal seagrass meadows as a result of observation improvements in terms of number of sites, spatial coverage and resolution, temporal frequency length of time-series, and seagrass metric consistency. First, EO can provide an historical baseline of seagrass indicators in the absence of *in situ* data (Knudby et al., 2010; León-Pérez et al., 2019), and provide updated information on seagrass status in many sites worldwide (Unsworth et al., 2019). In Europe, EO long-term and updated time-series could also help to select the year used as reference for the computation of the EQR within the WFD. Second, EO monitoring can be a cost-effective option to complement field data and overcome uncertainties related to the representativeness of sampling location or to the replication effort. Factors related to the spatial scale of sampling are indeed a major source of uncertainty in field assessments of ecological status, and it is recommended to prioritize large spatial replication over temporal replication (Mascaró et al., 2013). Seagrass density estimation based solely on field measurements depends on sampling strategies, and the number of replicates required to avoid undersampling of large seagrass meadows can be considerable and highly cost-effort demanding. Third, EO provides high-frequency observations. The highly dynamic nature of seagrass ecosystems calls for frequent monitoring. While the requirements of the WFD can be achieved with a single survey every ~ 6 years (Wilkes et al., 2017), EO makes it possible to acquire ~ yearly seagrass data thus significantly improving water quality monitoring within the WFD (Brito et al., 2020). In order to assess the influence of the temporal resolution, we reprocessed the EO time-series with a 6-year interval. The decadal increasing trend was still detectable, but the interannual variability was missed, and several maxima and minima were lost. Moreover, satellite observations can be incorporated into automatic processing chains to rapidly compute the seagrass status within hours after image acquisition, providing a broad spatial view of the ecosystem and allowing near real time seagrass monitoring. Fourth, EO makes it possible to quantitatively compare several metrics currently in use by EU Member States for seagrass monitoring. Marbà et al. (2013) identified 49 seagrass indicators used in 42 monitoring programs. This diversity is due in differences in measurement approaches and sampling strategies, EQR definition, and criteria to select the year of reference (Mascaró et al., 2013; Neto et al., 2018). Providing a consistent, Pan-European estimation of seagrass status require challenging intercalibration exercises (Foden, 2007; Neto et al., 2018). EO could help addressing such issue by providing a standardized, robust and harmonized framework for seagrass measurements (Papathanasopoulou et al., 2019). Importantly, the uncertainties associated to satellite estimations of the seagrass percent cover showed a negligible impact on the ecological status (Appendix C). Our preliminary assessment of the WFD seagrass metrics used in 3 different EU countries showed that the EQR method used in Portugal provided a higher estimation of the seagrass ecological status. In comparison, the EQRs used in France and UK were more conservative, did not show statistical difference of the ecological status, and are therefore comparable.

Satellite-based estimations, however, have inherent limitations. Field measurements are essential to validate satellite data, and to monitor seagrass colonization in new places, especially in areas with scattered seagrass plants (SPC between 5 and 20%) where satellite observations are subjected to some uncertainties (Barillé et al., 2010). Low coverage areas are particularly important for seagrass restoring programs and for the modelling of seagrass expansion (Matheson et al., 2017). Furthermore, several seagrass parameters cannot be measured by remote-sensing, and require field sampling: *e.g.,* species identification, genetic diversity, above-

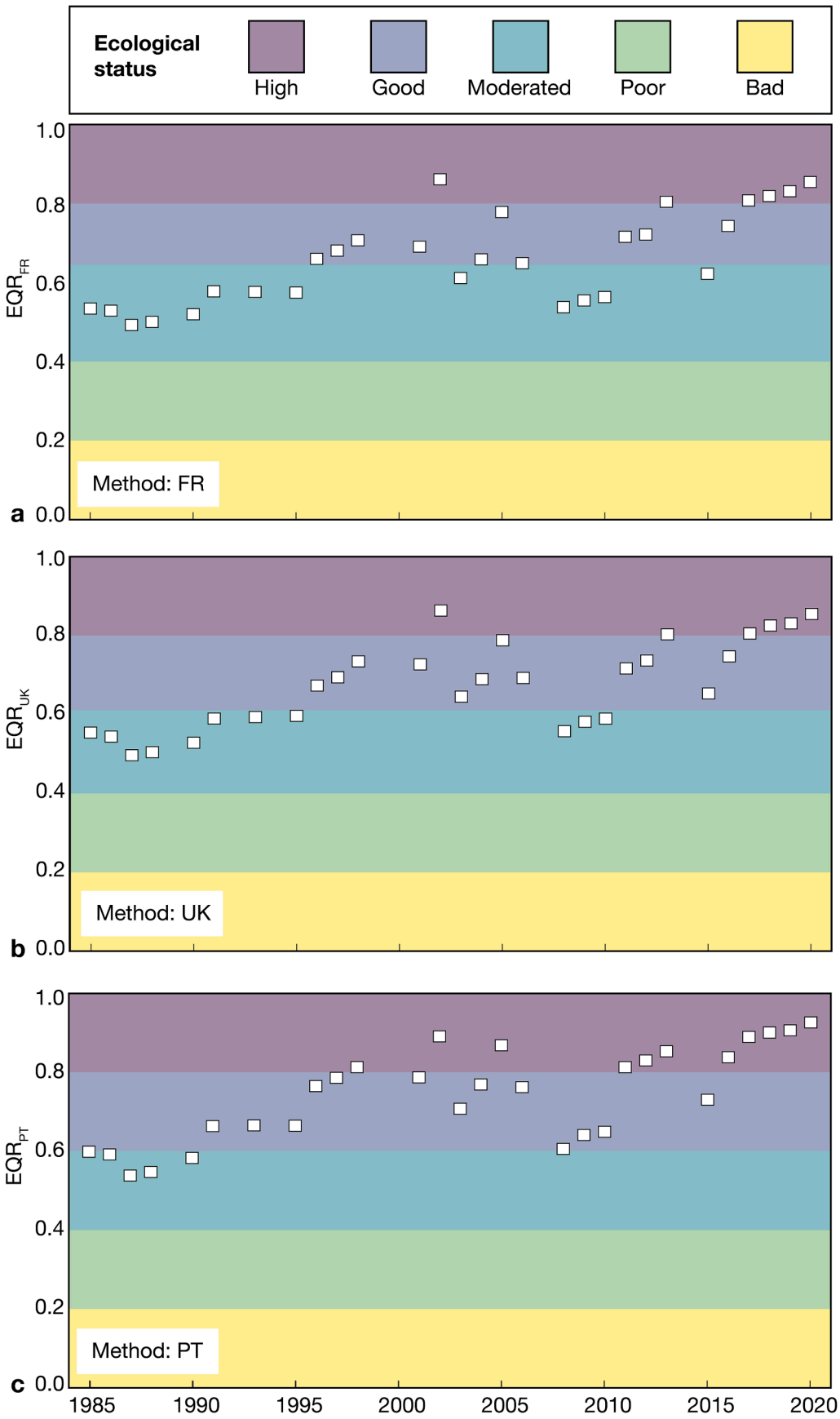

Fig. 8. Satellite-derived time series of seagrass ecological quality ratio (EQR) and ecological status (*sensu* the WFD) in Bourgneuf Bay from 1985 to 2020, using the French (a), British (b) and Portuguese (c) methods.

and below-ground biomass, presence of seed banks and epiphytic microalgae biomass. Finally, small seagrass meadows can remain undetected by remote-sensing due to limitation in spatial resolution. Commercial satellites with very high spatial resolution, as well as airborne or unmanned aerial vehicles (UAV) images still remain a viable option for small meadows where the pixel size offered by Landsat (30 m) or S2 (10 m) is too coarse, or for sites where the acquisition time is not adapted to the tidal constraints (Adolph et al., 2017; Duffy et al., 2018; Sousa et al., 2019; Zoffoli et al., 2020). Further research is also required for upscaling site-specific and/or species-specific radiometric methods to large-scale studies. While the SPC algorithm used in the present study to compute seagrass cover was calibrated in several macrotidal seagrass meadows dominated by *Z. noltei* along the European Atlantic coast and validated in Bourgneuf Bay (Zoffoli et al., 2020), the method needs to be validated in other sites prior to a broader application. Machine learning classification algorithms and Object-based Image Analysis (OBIA), have been tested to map intertidal seagrass. Martin (2020) showed that Random Forest provided the best results and that classifications were not improved by including variables obtained from OBIA. Machine learning methods can be adapted to map intertidal vegetation exploiting the 10 bands of S2 (Oiry and Barillé, 2020), but are likely less efficient with the reduced number of spectral bands of SPOT and Landsat. Ideally, seagrass mapping should combine new technologies (*e.g.,* UAV, satellites) with traditional *in situ* approaches (Unsworth et al., 2019). Despite some limitations, the advent of the S2 mission opens new perspectives, with high revisit time that increases the probabilities of having exploitable images and a mission lifetime predicted to be at least 15 years from 2015 that will permit seagrass time-series to be initiated or continued in time, at no-cost, and in many places of the world (Drusch et al., 2012; Traganos and Reinartz, 2018b).

4.2. Seagrass temporal variability in Bourgneuf Bay

In a climate-changing world, documenting long-term changes in seagrass density and spatial extent is relevant for ecosystems and biodiversity studies (El-Hacen et al., 2020) and for carbon budget modelling (McKenzie et al., 2020). In Bourgneuf Bay, an increase in seagrass extent has been previously documented from 1991 to 2005 (Barillé et al., 2010). The present study confirmed the recovery, expansion and overall good status of the seagrass meadow over the last 36 years. While seagrass have been globally declining (Dunic et al., 2021; Orth et al., 2006; Waycott et al., 2009; Xu et al., 2021) and experiencing catastrophic losses since the 19th century due to human impacts (Green et al., 2021), an increasing trend occurred in several European seagrass meadows in the 2000s (Calleja et al., 2017; de los Santos et al., 2019; Godet et al., 2008; Reise and Kohlus, 2008; Sousa et al., 2019). The net gain in seagrass area observed in Bourgneuf Bay since 1985 (2.7% yr^{-1}) is comparable with previously reported rates of change for *Z. noltei* in other European sites over the last two decades (de los Santos et al., 2019; Sousa et al., 2019). Several factors have been mentioned as responsible for this expansion. In the Wadden Sea, it was attributed to a higher sediment stability caused by a reduction in the number of storms since 1995 (Reise and Kohlus, 2008). De los Santos et al. (2019) suggested that the 2000s reversal trend in *Z. noltei* and *Z. marina* might be related to improvements in water quality and reduction of eutrophication rates, while a natural adjustment of the intertidal seagrass to past human impacts (namely large-scale dredging activities) was pointed out in Sousa et al. (2019). Román et al. (2020) also mentioned the reduction of shellfish harvesting among the regional factors responsible for a local seagrass increase. In this study, the highest seagrass density was observed in 2020, and coincides with a stop of shellfish harvesting due to a national lockdown in response to Covid-19 pandemic. However, the causality remains to be established. The identification of anthropogenic and environmental factors driving seagrass temporal variability in Bourgneuf Bay is out of scope of the present study, and will be investigated in future works.

Beside an overall increase, the seagrass time-series in Bourgneuf Bay exhibited a high-degree of interannual variability. Temporal fluctuations or "wax and wane" dynamics in extension and density metrics are frequent in seagrass ecosystems (*e.g.,* Calleja et al., 2017; Philippart and Dijkema, 1995; Reise and Kohlus, 2008; Valle et al., 2013; van Katwijk et al., 2006). The phases of decline and recovery displayed different dynamics. While the declines were generally abrupt, the recovering process was slower and progressive, suggesting a situation of hysteresis (Dolch et al., 2013; Neto et al., 2013), even for a fast-recovering *Zostera* species (Duarte et al. 2006; Godet et al., 2008; Matheson et al., 2017). Similarly, a study of decadal changes in Santander Bay (Spanish Atlantic coast) documented an overall increase in seagrass extent from 1984 to 2015, with episodic declines in 2003 and 2014–2015 (Calleja et al., 2017). The timing of the seagrass losses observed in northern Spain matched several declining events in Bourgneuf Bay, suggesting the possible influence of large-scale environmental factors on intertidal seagrass meadows. In particular, an extreme summer heat wave in 2003 was pointed out as the cause of a massive death event in several seagrass beds in Europe, including sites dominated by *Z. noltei* (Reusch et al., 2005; Ehlers et al., 2008; Zipperle et al., 2009).

In addition to long-term view, satellite images provided information of the seagrass bed spatial structure, such as the identification of large persistent spatial kernels. The resilience of such areas has been explained by a combination of sexual and clonal reproduction in other intertidal beds (Dolch et al., 2013). Their broad size could explain the recovering success of the seagrass meadow in Bourgneuf Bay. The rate of survival is generally higher in larger than smaller patches due to wave attenuation and resistance to sediment deposition (Inglis, 2000). Perennial seagrass kernels likely correspond to the location of flat and stable areas, coinciding with spatial patterns previously documented in other intertidal meadows (Dolch et al., 2013; Reise and Kohlus, 2008; Valle et al., 2013). On the contrary, intermittent seagrass patches likely correspond to high energy areas where seagrass recruitment capacity is impacted by wave erosion, or to areas impacted by sediment deposition (Fonseca and Kenworthy, 1987). Spatial analysis of seascape dynamics such as habitat losses and fragmentation could be useful to improve the management of seagrass meadows (Santos et al., 2016) by establishing priorities for site protection, assisting in restoration projects, identifying the best spots to perform reintroduction activities (Matheson et al., 2017), designing conservation policies and planning territorial organization (*e.g.,* permissions for oyster-farming activities around the meadow).

4.3. Consistency of satellite time-series

In the present study, the estimation of seagrass percent cover (SPC) and of subsequent metrics and indicators was based on satellite NDVI. It was therefore primordial to verify that the NDVI time-series was temporally stable and unbiased. While the combination of several satellite missions allowed us to increase the number of available observations, notably before the S2 era, cautious selection and processing steps were required to insure the temporal consistency of the multi-mission time-series (Maritorena and Siegel, 2005). Image selection was essential to avoid biases caused by seasonal and tidal variability (Zoffoli et al., 2020). The similar characteristics of Landsat, SPOT and S2 in terms of acquisition time, spectral and spatial resolutions favored the creation of an inter-calibrated NDVI time-series (Barnes et al., 2014). The differences in the position and width of the sensor's spectral bands were corrected to be compatible with S2 spectral response (Zoffoli et al., 2020). Despite the recalibration of the Landsat-derived NDVI, a remaining offset between $NDVI_{Landsat}$ and $NDVI_{SPOT/S2}$ persisted. While the temporal lag was reduced to a minimum for the matchup exercise, variation in atmospheric composition, sun elevation, viewing angles and environmental factors such as soil humidity or microphytobenthos could explain the differences between the satellite measurements. The systematic underestimation of Landsat compared to SPOT and S2, however, suggested that difference in atmospheric correction was the main source of discrepancy and the reason why we applied an offset correction to $NDVI_{Landsat}$ to achieve full consistency. The same atmospheric correction

(SMAC) was applied to SPOT and S2, and validated with an accuracy of approximately 16% in terms of NDVI. Though the LEDAPS atmospheric correction routinely performed for the Landsat dataset has been extensively validated over large continental areas, it might not be optimal for coastal zones (Nazeer et al., 2014). While cautious *in situ* validation, intercalibration and offset correction allowed us to consistently create a merged Landsat, SPOT and S2 time-series to analyze seagrass long-term changes in our study site, future work should address the challenge of reprocessing historical datasets to construct global continuous satellite records (Barnes et al., 2014; Fisher and Mustard, 2007).

5. Conclusions

In Bourgneuf Bay, the intertidal *Z. noltei*-dominated seagrass meadow has been in good or high status since the mid-1990s. Both the seagrass extent and meadow-averaged density showed an increasing trend from 1985 to 2020, superimposed over significant interannual fluctuations. The analysis of the meadow spatial distribution revealed different levels of fragmentation, with the existence of quasi-perennial seagrass kernels potentially coinciding with bathymetric optimum. By documenting the spatiotemporal dynamics of an intertidal seagrass in the frame of the WFD, this study aimed at demonstrating the efficiency of EO for seagrass monitoring in terms of temporal coverage, spatial resolution, and metric consistency.

Funding

This project has received funding from the European Union's Horizon 2020 research and innovation programme (Grant agreement n° 776348 – CoastObs).

Credit authorship contribution statement

Maria Laura Zoffoli: Conceptualization, Data curation, Formal analysis, Methodology, Investigation, Writing – original draft. **Pierre Gernez:** Conceptualizaton, Methodology, Investigation, Funding acquisition, Project administration, Writing – original draft. **Laurent Godet:** Formal analysis, Writing – review & editing. **Steef Peters:** Funding acquisition, Project administration, Writing – review & editing. **Simon Oiry:** Data curation, Writing – review & editing. **Laurent Barillé:** Conceptualizaton, Methodology, Investigation, Funding acquisition, Project administration, Writing – original draft.

Declaration of Competing Interest

The authors declare that they have no known competing financial interests or personal relationships that could have appeared to influence the work reported in this paper.

Acknowledgments

The European Space Agency (ESA), the United State Geological Service (USGS) and the *Centre National D'études Spatiales* (CNES) are acknowledged for the acquisition and provision of satellite data. The authors also thank Dr. Olivier Hagolle (CESBIO, France) for sharing the code of atmospheric correction for SPOT and Sentinel-2 data. Thank you to anonymous reviewers for their suggestions to improve our manuscript.

Appendix A

Characterization of seasonal variability

To perform consistent interannual analysis, only images acquired during the seasonal maximum of the seagrass development were used. A composite seasonal cycle was obtained using all Landsat5, 7 and 8 images acquired from 1984–2019, during low-tide and cloud-free conditions over Bourgneuf Bay. A dataset of 238 images was downloaded from the ESPA/USGS service as NDVI product ($NDVI_{Landsat}$). For each year, summer images were used to manually select the position of the densest seagrass pixels (8–20 pixels). The same pixels were extracted for the rest of the corresponding year. All data from 1984–2019 were combined in a single composite year from which weekly NDVI averages were calculated. A Gaussian function was fitted ($f(t) = a \bullet e^{(-((t-b)/c)^2)}$, $R^2 = 0.90$, p-value < 0.05), and used to determine the timing and temporal window of the seasonal maximum. The period of seagrass maximum, which was defined as the dates when NDVI remained within 5% of the maximum, was from 9/Aug–2/Oct ± 3.5 days (Fig. A1). We expanded the time boundaries for image acquisition to 26/Jul–15/Oct, allowing the inclusion of 5 additional years of data. However, we identified those 5 particular years as they would be subject to a temporal bias.

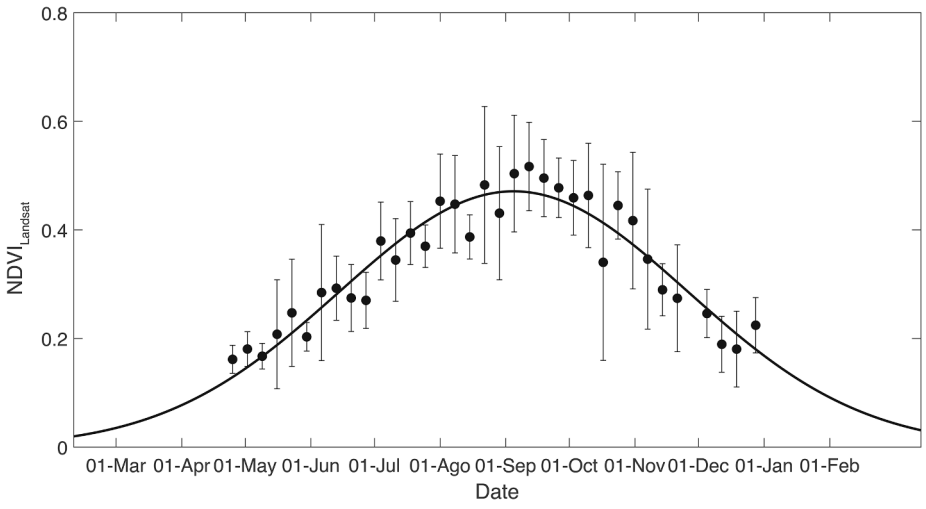

Fig. A1. *Z. noltei* seasonal cycle estimated from weekly NDVI averages from 1984–2019, in Bourgneuf Bay.

Appendix B

Long merged time-series: analysis of consistency

The SPOT/S2 and Landsat datasets (Table B1) were compared over four common types of intertidal landscapes: seagrass, bare sediment, sandy beach and macroalgae. Between 10- and 20-pixel samples were randomly extracted over each type of target. The extracted seagrass samples corresponded to the highest NDVI over the meadow. The sediment pixels were extracted over intertidal channels or close to the shoreline, where seagrass do not growth. The sand pixels were extracted along the beach in the southern side of the Noirmoutier Island. The macroalgae pixels were extracted over a permanently dense cover of macroalgae occupying an intertidal rocky shore in Bourgneuf Bay, north to the seagrass meadow.

Table B1
Details of the 29-image merged time-series (from SPOT, S2 and Landsat satellites) acquired over Bourgneuf Bay and used to evaluate interannual variability and trends. * marks indicate the dates that exceeded the maximum period of seagrass growth.

Year	Satellite	Day
1985	Landsat5	13 Sep.
1986	Landsat5	2 Oct.
1987	Landsat5	26 Jul.*
1988	SPOT1	15 Oct.*
1990	Landsat5	4 Sep.
1991	SPOT2	28 Aug.
1993	SPOT2	20 Aug.
1995	Landsat5	11 Oct.*
1996	SPOT2	16 Sep.
1997	SPOT1	7 Sep.
1998	SPOT1	21 Sep.
2001	Landsat5	2 Sep.
2002	SPOT5	24 Sep.
2003	SPOT5	26 Sep.
2004	Landsat7	17 Sep.
2005	SPOT5	18 Sep.
2006	Landsat5	23 Sep.
2008	Landsat5	28 Sep.
2009	SPOT5	8 Sep.
2010	SPOT5	12 Sep.
2011	SPOT5	2 Oct.
2012	SPOT4	28 Sep.
2013	SPOT5	5 Oct.*
2015	S2A	30 Sep.
2016	S2A	22 Aug.
2017	S2A	6 Oct.*
2018	S2A	14 Sep.
2019	S2A	16 Sep.
2020	S2B	5 Sep.

Appendix C

Assessing the influence of satellite measurement uncertainties on the estimation of indicator and status

In a previous work, the accuracy of the satellite measurement of seagrass percent cover was estimated to 14% using an extensive *in situ* validation dataset (Zoffoli et al., 2020). A random noise of 14% was therefore added to the *E* and *D* metrics to assess the influence of satellite measurement uncertainties on seagrass status (Fig. C1). Overall, the seagrass ecological status was robust to the addition of random uncertainties with only 3 or 4 years of difference in the ecological status.

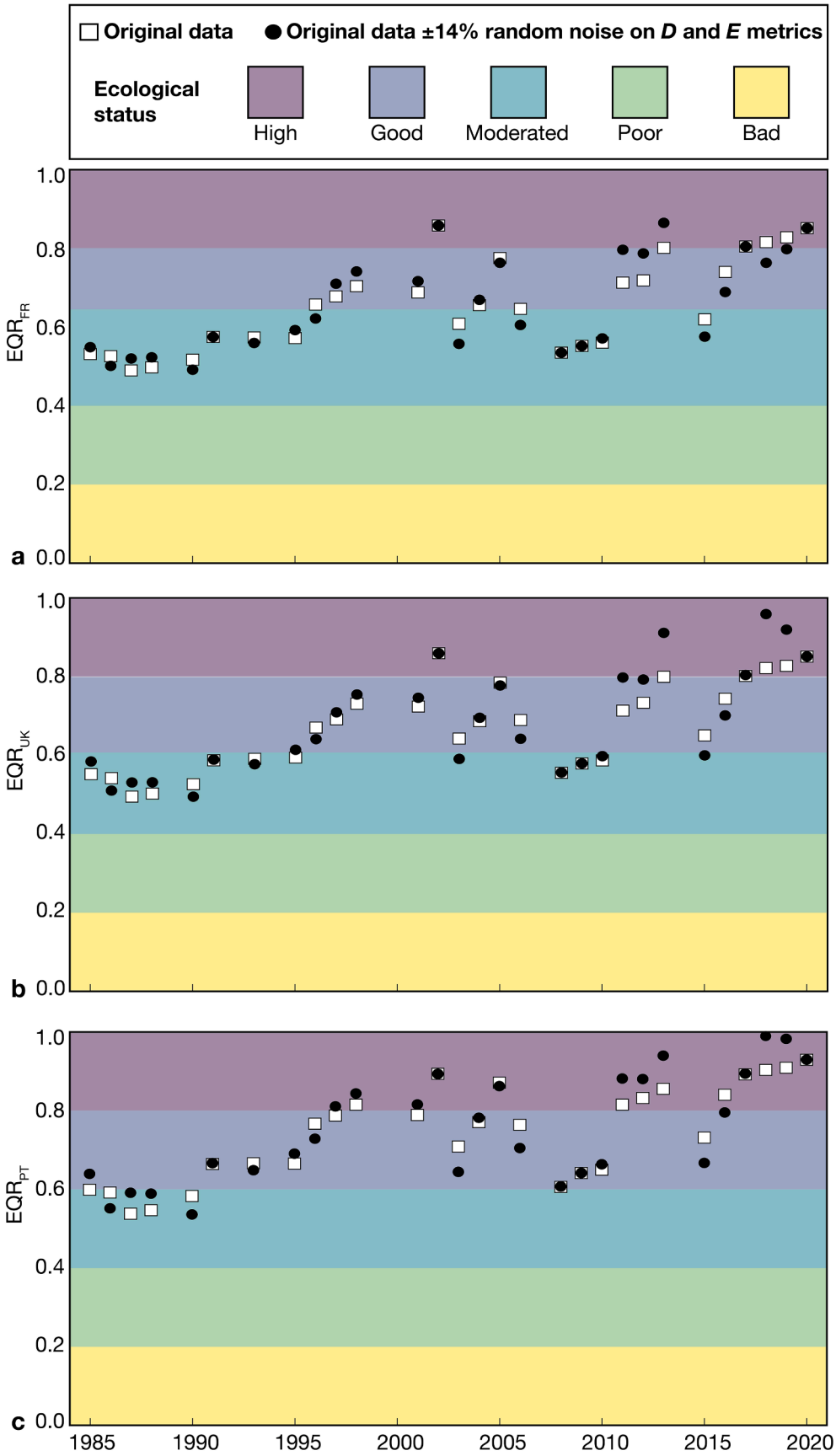

Fig. C1. Satellite-derived time series of seagrass ecological quality ratio (EQR) and ecological status (*sensu* the WFD) in Bourgneuf Bay from 1985–2020, using the French (a), British (b) and Portuguese (c) methods. White squares correspond to original data, while black dots refer to NDVI data with ± 14% of random uncertainties.

References

Adolph, W., Jung, R., Schmidt, A., Ehlers, M., Heipke, C., Bartholomä, A., Farke, H., 2017. Integration of TerraSAR-X, RapidEye and airborne lidar for remote sensing of intertidal bedforms on the upper flats of Norderney (German Wadden Sea). Geo-Mar. Lett. 37 (2), 193–205. https://doi.org/10.1007/s00367-016-0485-z.

Aljahdali, M.O., Munawar, S., Khan, W.R., 2021. Monitoring mangrove forest degradation and regeneration: Landsat time series analysis of moisture and vegetation indices at Rabigh Lagoon, red sea. Forests 12, 1–19. https://doi.org/10.3390/f12010052.

Auby, I., Oger-Jeanneret, H., Gouillieux, B., Grall, J., Janson, A.-L., Maguer, M., Rigouin, L., Rollet, C., Guy Sauriau, P., Trut, G., 2018. Protocoles suivi stationnel des herbiers à zostères pour la Directive Cadre sur l'Eau (DCE) Zostera marina - Zostera noltei. Version 3.

Bargain, A., 2012. Etude de la structure et de la dynamique des herbiers de Zostera noltii par télédétection multi et hyperspectrale. Université de Nantes.

Barillé, L., Robin, M., Harin, N., Bargain, A., Launeau, P., 2010. Increase in seagrass distribution at Bourgneuf Bay (France) detected by spatial remote sensing. Aquat. Bot. 92 (3), 185–194. https://doi.org/10.1016/j.aquabot.2009.11.006.

Barnes, B.B., Hu, C., Holekamp, K.L., Blonski, S., Spiering, B.A., Palandro, D., Lapointe, B., 2014. Use of Landsat data to track historical water quality changes in Florida Keys marine environments. Remote Sens. Environ. 140, 485–496. https://doi.org/10.1016/j.rse.2013.09.020.

Bertelli, C.M., Robinson, M.T., Mendzil, A.F., Pratt, L.R., Unsworth, R.K.F., 2018. Finding some seagrass optimism in Wales, the case of *Zostera noltii*. Mar. Pollut. Bull. 134, 216–222. https://doi.org/10.1016/j.marpolbul.2017.08.018.

Brito, A.C., Benyoucef, I., Jesus, B., Brotas, V., Gernez, P., Mendes, C.R., Launeau, P., Dias, M.P., Barillé, L., 2013. Seasonality of microphytobenthos revealed by remote-sensing in a South European estuary. Cont. Shelf Res. 66, 83–91. https://doi.org/10.1016/j.csr.2013.07.004.

Brito, A.C., Garrido-Amador, P., Gameiro, C., Nogueira, M., Moita, M.T., Cabrita, M.T., 2020. Integrating in situ and ocean color data to evaluate ecological quality under the water framework directive. Water 12, 3443. https://doi.org/10.3390/w12123443.

Calleja, F., Galvan, C., Silio-Calzada, A., Juanes, J.A., Ondiviela, B., 2017. Long-term analysis of Zostera noltei: a retrospective approach for understanding seagrasses' dynamics. Mar. Environ. Res. 130, 93–105. https://doi.org/10.1016/j.marenvres.2017.07.017.

Chai, B., Li, P., 2018. Annual urban expansion extraction and spatio-temporal analysis using landsat time series data: a case study of tianjin. IEEE J. Sel. Top. Appl. Earth Obs. Remote Sens. 11, 2644–2656. https://doi.org/10.1109/JSTARS.2018.2829525.

de los Santos, C.B., Krause-Jensen, D., Alcoverro, T., Marbà, N., Duarte, C.M., van Katwijk, M.M., Pérez, M., Romero, J., Sánchez-Lizaso, J.L., Roca, G., Jankowska, E., Pérez-Lloréns, J.L., Fournier, J., Montefalcone, M., Pergent, G., Ruiz, J.M., Cabaço, S., Cook, K., Wilkes, R.J., Moy, F.E., Trayter, G.-R., Arañó, X.S., de Jong, D. J., Fernández-Torquemada, Y., Auby, I., Vergara, J.J., Santos, R., 2019. Recent trend reversal for declining European seagrass meadows. Nat. Commun. 10 (1) https://doi.org/10.1038/s41467-019-11340-4.

Dekker, A.G., Brando, V.E., Anstee, J.M., 2005. Retrospective seagrass change detection in a shallow coastal tidal Australian lake. Remote Sens. Environ. 97 (4), 415–433. https://doi.org/10.1016/j.rse.2005.02.017.

Dolch, T., Buschbaum, C., Reise, K., 2013. Persisting intertidal seagrass beds in the northern Wadden Sea since the 1930s. J. Sea Res. 82, 134–141. https://doi.org/10.1016/j.seares.2012.04.007.

Dolch, T., Folmer, E. O., Frederiksen, M. S., Herlyn, M., van Katwijk, M. M., Kolbe, K., Krause-Jensen, D., Schemedes, P., Westerbeek, E. P., 2017. Wadden Sea Quality Status Report.

Drusch, M., Del Bello, U., Carlier, S., Colin, O., Fernandez, V., Gascon, F., Hoersch, B., Isola, C., Laberinti, P., Martimort, P., Meygret, A., Spoto, F., Sy, O., Marchese, F., Bargellini, P., 2012. Sentinel-2: ESA's optical high-resolution mission for GMES operational services. Remote Sens. Environ. 120, 25–36. https://doi.org/10.1016/j.rse.2011.11.026.

Duarte, C.M., Fourqurean, J.W., Krause-Jensen, D., Olesen, B., 2006. Dynamics of seagrass stability and change. In: Larkum, A.W.D., Orth, R.J., Duarte, C.M. (Eds.), Seagrasses: biology, ecology and conservation. Springer, Dordrecht, pp. 271–294.

Duffy, J.P., Pratt, L., Anderson, K., Land, P.E., Shutler, J.D., 2018. Estuarine, Coastal and Shelf Science Spatial assessment of intertidal seagrass meadows using optical imaging systems and a lightweight drone. Estuar. Coast. Shelf Sci. 200, 169–180. https://doi.org/10.1016/j.ecss.2017.11.001.

Dunic, J.C., Brown, C.J., Connolly, R.M., Turschwell, M.P., Côté, I.M., 2021. Long-term declines and recovery of meadow area across the world's seagrass bioregions. Glob. Change Biol. https://doi.org/10.1111/gcb.15684.

Ehlers, A., Worm, B., Reusch, T.B.H., 2008. Importance of genetic diversity in eelgrass *Zostera marina* for its resilience to global warming. Mar. Ecol. Prog. Ser. 355, 1–7. https://doi.org/10.3354/meps07369.

El Mahrad, B., Newton, A., Icely, J. D., Kacimi, I., Abalansa, S., Snoussi, M. (2020). Contribution of remote sensing technologies to a holistic coastal and marine environmental management framework: A review. Remote Sens. 12, 2313. 10.3390/rs12142313.

El-Hacen, E.H.M., Sidi Cheikh, M.A., Bouma, T.J., Olff, H., Piersma, T., 2020. Long-term changes in seagrass and benthos at Banc d'Arguin, Mauritania, the premier intertidal system along the East Atlantic Flyway. Glob. Ecol. Conserv. 24, e01364. https://doi.org/10.1016/j.gecco.2020.e01364.

Fisher, J.I., Mustard, J.F., 2007. Cross-scalar satellite phenology from ground, Landsat, and MODIS data. Remote Sens. Environ. 109 (3), 261–273. https://doi.org/10.1016/j.rse.2007.01.004.

Foden, J.o., 2007. Assessment metrics for littoral seagrass under the European Water Framework Directive; outcomes of UK intercalibration with the Netherlands. Hydrobiologia 579 (1), 187–197. https://doi.org/10.1007/s10750-006-0402-y.

Foden, J.o., Brazier, D.P., 2007. Angiosperms (seagrass) within the EU water framework directive: A UK perspective. Mar. Pollut. Bull. 55 (1-6), 181–195. https://doi.org/10.1016/j.marpolbul.2006.08.021.

Fonseca, M.S., Kenworthy, W.J., 1987. Effects of current on photosynthesis and distribution of seagrasses. Aquat. Bot. 27 (1), 59–78. https://doi.org/10.1016/0304-3770(87)90086-6.

Froidefond, J.M., Lafon, V., de Montaudouin, X., 2012. Variations saisonnière et annuelle de l'indice NDVI en relation avec les herbiers de zostères (*Zostera noltii*) par images satellites SPOT: exemple du bassin d'Arcachon (France). Rev. Francaise de Photogramm. et de Teledetection 197, 52–62.

Gernez, P., Barillé, L., Lerouxel, A., Mazeran, C., Lucas, A., Doxaran, D., 2014. Remote sensing of suspended particulate matter in turbid oyster-farming ecosystems. J. Geophys. Res. 119 (10), 7277–7294. https://doi.org/10.1002/2014JC010055.

Godet, L., Fournier, J., Jaffré, M., Desroy, N., 2011. Influence of stability and fragmentation of a worm-reef on benthic macrofauna. Estuar. Coast. Shelf Sci. 92 (3), 472–479. https://doi.org/10.1016/j.ecss.2011.02.003.

Godet, L., Fournier, J., Van Katwijk, M.M., Olivier, F., Le Mao, P., Retière, C., 2008. Before and after wasting disease in common eelgrass *Zostera marina* along the French Atlantic coasts: A general overview and first accurate mapping. Dis. Aquat. Org. 79, 249–255. https://doi.org/10.3354/dao01897.

Green, A.E., Chadwick, M.A., Jones, P.J.S., Green, A.E., 2021. Historical Analysis Exposes Catastrophic Seagrass Loss for the United Kingdom. Front. Plant Sci. 12, 629962. https://doi.org/10.3389/fpls.2021.629962.

Gruet, Y., 1976. Répartition des herbiers de Zostera (Monocotylédones marines) sur l'estran des côtes de Loire-Atlantique et du nord de la Vendée. Bull. Soc. Sci. Nat. Ouest Fr. 74, 86–90.

Hagolle, O., Sylvander, S., Huc, M., Claverie, M., Clesse, D., Dechoz, C., Lonjou, V., Poulain, V., 2015. SPOT-4 (Take 5): Simulation of Sentinel-2 time series on 45 large sites. Remote Sens. 7, 12242–12264. https://doi.org/10.3390/rs70912242.

Hossain, M.S., Bujang, J.S., Zakaria, M.H., Hashim, M., 2015. The application of remote sensing to seagrass ecosystems: an overview and future research prospects. Int. J. Remote Sens. 36 (1), 61–114. https://doi.org/10.1080/01431161.2014.990649.

Inglis, G.J., 2000. Variation in the recruitment behaviour of seagrass seeds: implications for population dynamics and resource management. Pac. Conserv. Biol. 5, 251–259. https://doi.org/10.1071/PC000251.

Klemas, V., 2013. Remote sensing of emergent and submerged wetlands: an overview. Int. J. Remote Sens. 34 (18), 6286–6320. https://doi.org/10.1080/01431161.2013.800656.

Knudby, A., Newman, C., Shaghude, Y., Muhando, C., 2010. Simple and effective monitoring of historic changes in nearshore environments using the free archive of Landsat imagery. Int. J. Appl. Earth Obs. Geoinf. 12, S116–S122. https://doi.org/10.1016/j.jag.2009.09.002.

Kohlus, J., Stelzer, K., Müller, G., Smollich, S., 2020. Mapping seagrass (Zostera) by remote sensing in the Schleswig-Holstein Wadden Sea. Estuar. Coast. Shelf Sci. 238, 106699. https://doi.org/10.1016/j.ecss.2020.106699.

Kovacs, E., Roelfsema, C., Lyons, M., Zhao, S., Phinn, S., 2018. Seagrass habitat mapping: how do Landsat 8 OLI, Sentinel-2, ZY-3A, and Worldview-3 perform? Remote Sens. Lett. 9 (7), 686–695. https://doi.org/10.1080/2150704X.2018.1468101.

Kuo, Y.-M., Lin, H.-J., 2010. Dynamic factor analysis of long-term growth trends of the intertidal seagrass Thalassia hemprichii in southern Taiwan. Estuar. Coast. Shelf Sci. 86 (2), 225–236. https://doi.org/10.1016/j.ecss.2009.11.017.

León-Pérez, M.C., Hernández, W.J., Armstrong, R.A., 2019. Characterization and Distribution of Seagrass Habitats in a Caribbean Nature Reserve using High-Resolution Satellite Imagery and Field Sampling. J. Coast. Res. 35, 937–947. https://doi.org/10.2112/JCOASTRES-D-18-00106.1.

Lõugas, L., Kutser, T., Kotta, J., Vahtmäe, E., 2020. Detecting long time changes in benthic macroalgal cover using landsat image archive. Remote Sens. 12, 1901. https://doi.org/10.3390/rs12111901.

Lyons, M.B., Roelfsema, C.M., Phinn, S.R., 2013. Towards understanding temporal and spatial dynamics of seagrass landscapes using time-series remote sensing. Estuar. Coast. Shelf Sci. 120, 42–53. https://doi.org/10.1016/j.ecss.2013.01.015.

Marbà, N., Krause-Jensen, D., Alcoverro, T., Birk, S., Pedersen, A., Neto, J.M., Orfanidis, S., Garmendia, J.M., Muxika, I., Borja, A., Dencheva, K., Duarte, C.M., 2013. Diversity of European seagrass indicators: Patterns within and across regions. Hydrobiologia 704 (1), 265–278. https://doi.org/10.1007/s10750-012-1403-7.

Maritorena, S., Siegel, D.A., 2005. Consistent merging of satellite ocean color data sets using a bio-optical model. Remote Sens. Environ. 94 (4), 429–440. https://doi.org/10.1016/j.rse.2004.08.014.

Martin, R.D., 2020. Determining estuarine seagrass condition measures from low altitude multi-spectral imagery flown by remotely piloted aircraft. PhD Thesis. University of Waikato, New Zealand, p. 342 pp..

Mascaró, O., Alcoverro, T., Dencheva, K., Díez, I., Gorostiaga, J.M., Krause-Jensen, D., Balsby, T.J.S., Marbà, N., Muxika, I., Neto, J.M., Nikolić, V., Orfanidis, S., Pedersen, A., Pérez, M., Romero, J., 2013. Exploring the robustness of macrophyte-based classification methods to assess the ecological status of coastal and transitional ecosystems under the Water Framework Directive. Hydrobiologia 704, 279–291. https://doi.org/10.1007/s10750-012-1426-0.

Matheson, F.E., Reed, J., Dos Santos, V.M., Mackay, G., Cummings, V.J., 2017. Seagrass rehabilitation: successful transplants and evaluation of methods at different spatial scales. N. Z. J. Mar. Freshwater Res. 51 (1), 96–109. https://doi.org/10.1080/00288330.2016.1265993.

McKenzie, L.J., Nordlund, L.M., Jones, B.L., Cullen-Unsworth, L.C., Roelfsema, C., Unsworth, R.K.F., 2020. The global distribution of seagrass meadows. Environ. Res. Lett. 15 (7), 074041. https://doi.org/10.1088/1748-9326/ab7d06.

Méléder, V., Savelli, R., Barnett, A., Polsenaere, P., Gernez, P., Cugier, P., Lerouxel, A., Le Bris, A., Dupuy, C., Le Fouest, V., Lavaud, J., 2020. Mapping the Intertidal Microphytobenthos Gross Primary Production Part I: Coupling Multispectral Remote Sensing and Physical Modeling. Front. Mar. Sci. 7, 520. https://doi.org/10.3389/fmars.2020.00520.

Murphy, G.E.P., Dunic, J.C., Adamczyk, E.M., Bittick, S.J., Côté, I.M., Cristiani, J., Geissinger, E.A., Gregory, R.S., Lotze, H.K., O'Connor, M.I., Araújo, C.A.S., Rubidge, E.M., Templeman, N.D., Wong, M.C., 2021. From coast to coast to coast: ecology and management of seagrass ecosystems across Canada. Facets 6, 1–41. https://doi.org/10.1139/facets-2020-0020.

Nazeer, M., Nichol, J.E., Yung, Y.-K., 2014. Evaluation of atmospheric correction models and Landsat surface reflectance product in an urban coastal environment. Int. J. Remote Sens. 35 (16), 6271–6291. https://doi.org/10.1080/01431161.2014.951742.

Neto, J.M., Salas Herrero, F., Best, M., Buchet, R., Heiber, W., Juanes, J.A., Kolbe, K., Recio, M., Ruiter, H., Scanlan, C., Wilkes, R., 2018. Coastal and Transitional waters North East Atlantic geographic intercalibration group. Seagrasses Ecol. Assess. Methods. https://doi.org/10.2760/86847.

Neto, J.M., Barroso, D.V., Barría, P., 2013. Seagrass Quality Index (SQI), a Water Framework Directive compliant tool for the assessment of transitional and coastal intertidal areas. Ecol. Indic. 30, 130–137. https://doi.org/10.1016/j.ecolind.2013.02.015.

Oiry, S., Barillé, L., 2020. Using sentinel-2 satellite imagery to develop microphytobenthos-based water quality indices in estuaries. Ecol. Indic. 121, 107184. https://doi.org/10.1016/j.ecolind.2020.107184.

Orth, Robert J., Carruthers, Tim J.B., Dennison, William C., Duarte, Carlos M., Fourqurean, James W., Heck, Kenneth L., Hughes, A. Randall, Kendrick, Gary A., Kenworthy, W. Judson, Olyarnik, Suzanne, Short, Frederick T., Waycott, Michelle, Williams, Susan L., 2006. A Global Crisis for Seagrass Ecosystems. BioScience 56 (12), 987. https://doi.org/10.1641/0006-3568(2006)56[987:AGCFSE]2.0.CO;2.

Palandro, D.A., Andréfouët, S., Hu, C., Hallock, P., Müller-Karger, F.E., Dustan, P., Callahan, M.K., Kranenburg, C., Beaver, C.R., 2008. Quantification of two decades of shallow-water coral reef habitat decline in the Florida Keys National Marine Sanctuary using Landsat data (1984–2002). Remote Sens. Environ. 112 (8), 3388–3399. https://doi.org/10.1016/j.rse.2008.02.015.

Papathanasopoulou, E., Simis, S., Alikas, K., Ansper, A., Anttila, S., Attila, J., Barillé, A.-L., Barillé, L., Brando, V., Bresciani, M., Bučas, M., Gernez, P., Giardino, C., Harin, N., Hommerson, A., Kangro, K., Kauppila, P., Koponen, S., Laanen, M., Neil, C., Papadakis, D., Peters, S., Poikane, S., Poser, K., Pires, M. D., Riddick, C., Spyrakos, E., Tyler, A., Vaičiūtė, D., Warren, M., Zoffoli, M.L., 2019. Satellite-assisted monitoring of water quality to support the implementation of the Water Framework Directive (Version 1.0). EOMORES white paper. 10.5281/zenodo.3463051.

Philippart, C.J.M., Dijkema, K.S., 1995. Wax and wane of *Zostera noltii* Hornem. in the Dutch Wadden Sea. Aquat. Bot. 49 (4), 255–268. https://doi.org/10.1016/0304-3770(94)00431-K.

Phinn, S., Roelfsema, C., Dekker, A., Brando, V., Anstee, J., 2008. Mapping seagrass species, cover and biomass in shallow waters: An assessment of satellite multi-spectral and airborne hyper-spectral imaging systems in Moreton Bay (Australia). Remote Sens. Environ. 112 (8), 3413–3425. https://doi.org/10.1016/j.rse.2007.09.017.

RAHMAN, H., DEDIEU, G., 1994. SMAC: A simplified method for the atmospheric correction of satellite measurements in the solar spectrum. Int. J. Remote Sens. 15 (1), 123–143. https://doi.org/10.1080/01431169408954055.

Reise, K., Kohlus, J., 2008. Seagrass recovery in the Northern Wadden Sea? Helgol. Mar. Res. 62, 77–84. https://doi.org/10.1007/s10152-007-0088-1.

Reusch, T.B.H., Ehlers, A., Hammerli, A., Worm, B., 2005. Ecosystem recovery after climatic extremes enhanced by genotypic diversity. Proc. Natl. Acad. Sci. 102 (8), 2826–2831. https://doi.org/10.1073/pnas.0500008102.

Roelfsema, C.M., Lyons, M., Kovacs, E.M., Maxwell, P., Saunders, M.I., Samper-Villarreal, J., Phinn, S.R., 2014. Multi-temporal mapping of seagrass cover, species and biomass: A semi-automated object based image analysis approach. Remote Sens. Environ. 150, 172–187. https://doi.org/10.1016/j.rse.2014.05.001.

Román, M., Fernández, E., Zamborain-Mason, J., Martínez, L., Méndez, G., 2020. Decadal changes in the spatial coverage of *Zostera noltei* in two seagrass meadows (Ría de Vigo; NW Spain). Reg. Stud. Mar. Sci. 36, 101264. https://doi.org/10.1016/j.rsma.2020.101264.

Rudorff, N. de M., Kampel, M., Rezende, C. E., 2011. Spectral mapping of the Paraíba do Sul River plume (Brazil) using multitemporal Landsat images. J. Appl. Remote Sens. 5, 053550. 10.1117/1.3630220.

Sanchez, M., 2008. Dynamique des sédiments fins dans une zone côtière à forte turbidité à proximité de l'embouchure de la Loire. In: Xèmes Journées Nationales Génie Côtier – Génie Civil, 14-16 Octobre 2008, Sophia Antipolis, 169–178. 10.5150/jngcgc.2008.016-s.

Santos, Rolando O., Lirman, Diego, Pittman, Simon J., 2016. Long-term spatial dynamics in vegetated seascapes: Fragmentation and habitat loss in a human-impacted subtropical lagoon. Mar. Ecol. 37 (1), 200–214. https://doi.org/10.1111/maec.12259.

Santos, R. O., Varona, G., Avila, C. L., Lirman, D., Collado-Vides, L., 2020. Implications of macroalgae blooms to the spatial structure of seagrass seascapes: The case of the Anadyomene spp. (Chlorophyta) bloom in Biscayne Bay, Florida. Mar. Pollut. Bull. 150, 110742. 10.1016/j.marpolbul.2019.110742.

Shelton, Andrew O., Francis, Tessa B., Feist, Blake E., Williams, Gregory D., Lindquist, Adam, Levin, Philip S., Hughes, A. Randall, 2017. Forty years of seagrass population stability and resilience in an urbanizing estuary. J. Ecol. 105 (2), 458–470. https://doi.org/10.1111/jec.2017.105.issue-210.1111/1365-2745.12682.

Short, Frederick T., Wyllie-Echeverria, Sandy, 1996. Natural and human-induced disturbance of seagrasses. Environ. Conserv. 23 (1), 17–27. https://doi.org/10.1017/S0376892900038212.

Sousa, A.I., da Silva, J.F., Azevedo, A., Lillebø, A.I., 2019. Blue Carbon stock in *Zostera noltei* meadows at Ria de Aveiro coastal lagoon (Portugal) over a decade. Sci. Rep. 9, 1–13. https://doi.org/10.1038/s41598-019-50425-4.

Traganos, D., Reinartz, P., 2018a. Interannual Change Detection of Mediterranean Seagrasses Using RapidEye Image Time Series. Front. Plant Sci. 9, 96. https://doi.org/10.3389/fpls.2018.00096.

Traganos, D., Reinartz, P., 2018b. Mapping Mediterranean seagrasses with Sentinel-2 imagery. Mar. Pollut. Bull. 134, 197–209. https://doi.org/10.1016/j.marpolbul.2017.06.075.

Tucker, Compton J., 1979. Red and photographic infrared linear combinations for monitoring vegetation. Remote Sens. Environ. 8 (2), 127–150. https://doi.org/10.1016/0034-4257(79)90013-0.

UKTAG, 2014. UKTAG Transitional & Coastal Water Assessment Method - Angiosperm: Intertidal Seagrass Tool.

Unsworth, Richard K.F., McKenzie, Len J., Collier, Catherine J., Cullen-Unsworth, Leanne C., Duarte, Carlos M., Eklöf, Johan S., Jarvis, Jessie C., Jones, Benjamin L., Nordlund, Lina M., 2019. Global challenges for seagrass conservation. Ambio 48 (8), 801–815. https://doi.org/10.1007/s13280-018-1115-y.

Valle, M., Palà, V., Lafon, V., Dehouck, A., Garmendia, J.M., Borja, Á., Chust, G., 2015. Mapping estuarine habitats using airborne hyperspectral imagery, with special focus on seagrass meadows. Estuar. Coast. Shelf Sci. 164, 433–442. https://doi.org/10.1016/j.ecss.2015.07.034.

Valle, M., van Katwijk, M.M., de Jong, D.J., Bouma, T.J., Schipper, A.M., Chust, G., Benito, B.M., Garmendia, J.M., Borja, Á., 2013. Comparing the performance of species distribution models of *Zostera marina*: Implications for conservation. J. Sea Res. 83, 56–64. https://doi.org/10.1016/j.seares.2013.03.002.

van der Wal, Daphne, Wielemaker-van den Dool, Annette, Herman, Peter M.J., 2010. Spatial synchrony in intertidal benthic algal biomass in temperate coastal and estuarine ecosystems. Ecosystems 13 (2), 338–351. https://doi.org/10.1007/s10021-010-9322-9.

van Katwijk, M. M., Geerling, G. W., Rašín, R., van 't Veer, R., Bos, A. R., Hermus, D. C. R., van Wieringen, M., Jager, Z., Groeneweg, A., Erftemeijer, P. L. A., van der Heide, T., de Jong, D. J., 2006. Macrophytes in the western Wadden Sea: monitoring, invasion, transplantations, dynamics and European policy. In: Laursen, K.; Marencic, H. (Ed.), 11th International Scientific Wadden Sea Symposium, 4 - 8 April 2005, pp. 89–111.

Walker, D.I., McComb, A.J., 1992. Seagrass degradation in Australian coastal waters. Mar. Pollut. Bull. 25, 191–195. https://doi.org/10.1016/0025-326X(92)90224-T.

Water Framework Directive 2000/60/EC. European Communities Official Journal L327 22.12.2000, p. 73.

Waycott, M., Duarte, C.M., Carruthers, T.J.B., Orth, R.J., Dennison, W.C., Olyarnik, S., Calladine, A., Fourqurean, J.W., Heck, K.L., Hughes, A.R., Kendrick, G.A., Kenworthy, W.J., Short, F.T., Williams, S.L., 2009. Accelerating loss of seagrasses across the globe threatens coastal ecosystems. Proc. Natl. Acad. Sci. 106, 12377–12381. https://doi.org/10.1073/pnas.0905620106.

Wilkes, R., Bennion, M., McQuaid, N., Beer, C., McCullough-Annett, G., Colhoun, K., Inger, R., Morrison, L., 2017. Intertidal seagrass in Ireland: Pressures, WFD status and an assessment of trace element contamination in intertidal habitats using *Zostera noltei*. Ecol. Indic. 82, 117–130. https://doi.org/10.1016/j.ecolind.2017.06.036.

Xu, S., Xu, S., Zhou, Y., Yue, S., Zhang, X., Gu, R., Zhang, Y., Qiao, Y., Liu, M., 2021. Long-Term Changes in the Unique and Largest Seagrass Meadows in the Bohai Sea (China) Using Satellite (1974 – 2019) and Sonar Data: Implication for Conservation and Restoration. Remote Sens., 13, 856. 10.3390/ rs13050856.

Young, D., Clinton, P., Specht, D., Mochon Collura, T.C., 2015. Comparison of non-native dwarf eelgrass (*Zostera japonica*) and native eelgrass (*Zostera marina*) distributions in a northeast Pacific estuary: 1997–2014. Bot. Mar. 58, 239–250. https://doi.org/10.1515/bot-2014-0088.

Young, D., Clinton, P., Specht, D., Mochon Collura, T.C., Lee II, H., 2012. Determining bathymetric distributions of the eelgrass *Zostera marina* L. in three turbid estuaries on the eastern North Pacific coast. Bot. Mar. 55, 229–240. https://doi.org/10.1515/bot-2011-0011.

Zipperle, A.M., Coyer, J.A., Reise, K., Stam, W.T., Olsen, J.L., 2009. Evidence for persistent seed banks in dwarf eelgrass *Zostera noltii* in the German Wadden Sea. Mar. Ecol. Prog. Ser. 380, 73–80. https://doi.org/10.3354/meps07929.

Zoffoli, M.L., Gernez, P., Rosa, P., Le Bris, A., Brando, V.E., Barillé, A.L., Harin, N., Peters, S., Poser, K., Spaias, L., Peralta, G., Barillé, L., 2020. Sentinel-2 remote sensing of *Zostera noltei*-dominated intertidal seagrass meadows. Remote Sens. Environ 251, 112020. https://doi.org/10.1016/j.rse.2020.112020.